J Mol Model (2014) 20:2254
DOI 10.1007/s00894-014-2254-0

ORIGINAL PAPER

# Theoretical insight into the mechanism for the inhibition of the cysteine protease cathepsin B by 1,2,4-thiadiazole derivatives

**Mauricio Angel Vega-Teijido · Sarah El Chamy Maluf · Camila Ramalho Bonturi · Julio Ricardo Sambrano · Oscar N. Ventura**

Received: 28 February 2014 / Accepted: 21 April 2014 / Published online: 1 June 2014


**Abstract** Several cellular disorders have been related to the overexpression of the cysteine protease cathepsin B (CatB), such as rheumatic arthritis, muscular dystrophy, osteoporosis, Alzheimer's disease, and tumor metastasis. Therefore, inhibiting CatB may be a way to control unregulated cellular functions and prevent tissue malformations. The inhibitory action of 1,2,4-thiadiazole (TDZ) derivatives has been associated in the literature with their ability to form disulfide bridges with the catalytic cysteine of CatB. In this work, we present molecular modeling and docking studies of a series of eight 1,2,4-thiadiazole compounds. Substitutions at two positions (3 and 5) on the 1,2,4-thiadiazole ring were analyzed, and the docking scores were correlated to experimental data. A correlation was found with the sequence of scores of four related compounds with different substituents at position 5. No correlation was observed for changes at position 3. In addition, quantum chemistry calculations were performed on smaller molecular models to study the mechanism of inhibition of TDZ at the active site of CatB. All possible protonation states of the ligand and the active site residues were assessed. The tautomeric form in which the proton is located on N2 was identified as the species that has the structural and energetic characteristics that would allow the ring opening of 1,2,4-thiadiazole.

**Keywords** Cysteine protease · Cathepsin · Thiadiazole · Docking · Quantum chemistry

This paper belongs to Topical Collection QUITEL 2013

**Electronic supplementary material** The online version of this article (doi:10.1007/s00894-014-2254-0) contains supplementary material, which is available to authorized users.

M. A. Vega-Teijido (✉) · O. N. Ventura
Computational Chemistry and Biology Group—CCBG, DETEMA, Facultad de Química, Universidad de la República, CC1157, 11800 Montevideo, Uruguay
e-mail: mauryvg@gmail.com

S. El Chamy Maluf · C. R. Bonturi · J. R. Sambrano
Departamento de Matemática, Grupo de Modelagem e Simulação Molecular—GMSM, Universidade Estadual Paulista "Julio de Mesquita Filho", 17033-360 Bauru, São Paulo—SP, Brasil

## Introduction

Cysteine proteases comprise a broad superfamily of enzymes that are involved in the cellular process of protein degradation and are expressed in organisms ranging from bacteria to humans [1–5]. There are 11 known lysosomal papain-like cysteine proteases in humans, which are commonly termed "cathepsins" [1–5]. Detailed information on and the classification of these proteases can be accessed in the Merops database at http://merops.sanger.ac.uk [6, 7]. Cathepsins can be characterized as either exopeptidases (cathepsins C, H, and X) or endopeptidases (cathepsins B, L, S, V, F, K, and W) [4, 8]. Despite the fact that cathepsin B (CatB) is generally categorized as an endopeptidase, the presence of two His (110 and 111) units at the limit of sub-site S2′ has been associated with an ability to act as a C-terminal dipeptidase [2, 4, 5]. In this process, the flexible chain fragment known as the "occluding loop" has been reported to play a key role in the binding at the cleft of the active site [5, 9–11].

The catalytic mechanism of CatB involves a pre-activated thiolate form of Cys29 derived from the transfer of a proton to His199, which has its imidazolium ring stabilized by Asn219 [12, 13]. In the first step, the carbonyl of the peptide bond undergoes nucleophilic attack by the thiolate, resulting in a tetrahedral intermediate. Subsequently, the C-terminal peptide leaves the active site and a thioester simultaneously forms between Cys29 and the N-terminal fragment. The addition of a water molecule generates a second tetrahedral

intermediate, which finally undergoes a deacylation process that releases the N-terminal fragment and reconstitutes the ionic pair $Cys29^{(-)}$ /$His199^{(+)}$ [14].

CatB is responsible for many biological functions, including the degradation of connective tissue proteins [15] and extracellular matrix components such as collagen type IV, laminin, and fibronectin [16], and is involved in the activation of some proteins [15, 16]. Dysfunction of the biological mechanisms of CatB control can trigger some degenerative diseases such as rheumatoid arthritis [1], osteoporosis [2], multiple sclerosis [17, 18], muscular dystrophy [19], and pancreatitis [20]. In the last few years, CatB has been associated with the production of neurotoxic β-amyloid peptides that accumulate in Alzheimer's disease [21–23], bone metastasis in breast cancer [24], and carcinogenesis in colorectal cancer [25]. Recently, endosomal CatB was reported to be used subversively by the highly pathogenic Nipah virus to activate its fusion protein in the cell-to-cell infection process [26].

Inhibition of CatB under physiological conditions is observed specifically in peptides of the cystatin superfamily, which includes stefins, cystatins, and kininogens [5]. Regulation of the CatB activity of these peptides isachieved through tertiary structural modification of the occluding loop, during which the catalytic residues remain unaltered but access to the active site is impeded by the inhibitor [27]. The pH dependence of CatB activity and the stabilization of the enzyme were recently associated with an allosteric role of heparin [28].

Early reports have demonstrated that inhibition of CatB can result from the action of small active compounds at the active site [1–3]. Therefore, CatB has been considered a potential target for drug development. Several efforts have already been made to regulate CatB proteolytic activity using small inhibitors [29]. In general, the inhibitors tested showed a limited efficiency in vivo and/or exhibited toxicity [19, 30, 31]. Recently, the selectivity of cathepsins has been under study; for instance, differences in the network of hydrogen bonds between CatL, CatL2, CatB, CatK, and CatS have been investigated [32]. In new attempts to find specific inhibitors of CatB, 3D-QSAR methods have been applied to benzenesulfonyl-pyrazol-ester derivatives [33] and to screen a library of 6-substituted 4-benzylthio-1,3,5-triazin-2(1*H*)-one compounds [34]. Other inhibitors that have been proposed are ruthenium(II) derivatives [35], the antibiotic nitroxoline (a non-competitive inhibitor) [36], redox-active 4-aminophenol compounds [37], organotellurium compounds ([38, 39] and references therein), and a natural compound from the marine sponge *Crella* (*Yvesia*) *spinulata* [40].

In the work reported in the present paper, we describe the molecular modeling and theoretical study of a series of eight 1,2,4-thiadiazole derivatives taken from a paper by Leung-Toung et al. [41]. Compounds in this family can be used to modulate the activity and selectivity of the enzyme cathepsin B through substitution at position 3 or 5 on the thiadiazole ring. As an additional point of interest, the inhibition mechanism involves a series of structural changes involving the formation of a disulfide and concomitant ring opening. In this paper, we report the molecular modeling of ligands, docking studies of complexes, and quantum chemical calculations of models that were performed to gain further insight into the molecular mechanism associated with these inhibitory compounds.

## Materials and methods

### Docking calculations

Docking calculations were performed using the GOLD suite of programs [42–44], in which the initial fitness score selected to evaluate the ligand–protein affinity (GOLDScore) is based on the Tripos 5.2 force field [45]. The score is calculated as a summation of selected molecular mechanics terms:

$$\text{GOLDScore} = \sum E_{\text{H-bond}} + \sum E_{\text{ext-vdW}} + \sum E_{\text{int-vdW}} + \sum E_{int-\text{torsion}},$$

where $E_{\text{H-bond}}$ is the energy of the ligand–protein hydrogen bond, $E_{\text{ext-vdW}}$ is the energy of the ligand–protein van der Waals interaction, $E_{\text{int-vdW}}$ is the energy of the intraligand van der Waals interactions, and $E_{\text{int-torsion}}$ is the torsion energy of the ligand. All the docking calculations included two steps: an initial step using GOLDScore and then a step involving rescoring and selection using the ChemPLP (piecewise linear potential) equation. The details of the ChemPLP equation can be consulted in [46]. GOLDScore and ChemPLP values are presented as positive numbers, meaning that the affinity increases as the score increases.

The receptor structures were selected through systematic analysis of the active sites in 20 crystallographic structures of CatB deposited in the RCSB Protein Data Bank (PDB) [47]. The codes of the 20 files retrieved are: 1cpj, 1cte, 1the, 2ipp, 1csb, 1qdq, 1sp4, 1ito, 1huc, 2dc6, 2dc7, 2dc8, 2dc9, 2dca, 2dcb, 2dcc, 2dcd, 1gmy, 3cbk, and 3cbj. Seven interatomic distances were used to characterize the active site of CatB, (see the "Electronic supplementary material," ESM). In light of these measures, the structures were grouped into two sets, with 1gmy the representative structure for one set [48] and 2dcd the representative structure for the other [49]. Because of the similarity of the 2dcd epoxy dipeptide ligand to some of the ligands included in this study, 2dcd was the first structure selected for the docking calculations. At the start of the study, the 2dcd receptor was validated by repeating a docking calculation using the original epoxy ligand. This procedure was performed in order to determine the parameters for the calculation and to confirm that the molecular complex was

correctly reproduced by the calculated structure. The conformational search was done within a 10 Å sphere centered on the S atom of the catalytic Cys29. The evolutionary parameters used were: population size=100, selection pressure=1.1, island=5, and niche size=2. Cutoff distances were defined as 2.5 Å for H bonds and 4.0 Å for van der Waals contacts. All docking calculations were performed using the GOLD genetic algorithm (GA) and involved 100,000 genetic operations (ca. 47.5 % crossovers, 47.5 % mutations, and 5 % migrations). The procedure determined for 2dcd was reproduced in four other receptor structures: 2dca, 2dcb, 2dcc [49], and 1gmy [48].

The molecular complexes were selected sequentially in two stages. Firstly, 10 solutions from GA calculations were evaluated numerically and graphically and grouped into clusters. Secondly, the ligand with the most favorable score and conformation was used to seed a new docking calculation of 10 GA. This procedure was used to confirm the solution and to refine the scoring. These latter docking calculations were run with a scaffold constraint (with a weighting factor of 5) over the input structure [43]. After evaluating the 10 new solutions, the ligand–protein complex was finally selected. The ligands were submitted to an additional study of covalent docking into the 2dcd receptor in order to explore the conformational compatibility between the noncovalent and covalent poses in the active site of CatB. This procedure was done to obtain the structures of the ligands associated with both situations—before and after the reaction between the thiol and the TDZ ring—as a way to evaluate the conformational evolution of the ligand in the surroundings of the active site. In addition to the eight ligands of the series, compound (1) was docked in the tautomeric form T3 (see below).

### Molecular modeling of ligands and quantum chemical calculations

A series of eight compounds reported by Leung-Toung et al. [41] were modeled from scratch with the program Discovery Studio Visualizer [50] (Scheme 1). The 1,2,4-thiadiazole ring was first constructed and the geometry optimized using the MOPAC2009 [51] program and the PM6 [52] semiempirical method. Substituents were attached to the ring at the R1 and/or R2 positions, and the geometry of each structure was then optimized. In addition, two forms of structure (1) were modeled, (1a) and (1b), with the thiadiazole ring closed and opened, respectively. The (1b) form includes an additional sulfur atom representing the sulfur atom of Cys29, with which the ligand may react. This is a structural requirement for covalent docking calculations. The optimized models mentioned above were those used in the docking studies.

The final part of the work utilized the structures obtained from the docking process. A full quantum chemical study of reduced models of the ligand docked at the active site was performed. Initially, the catalytic triad Cys29, His199, and Asn219 (representative of the active site) were modeled. All atoms in the residues Cys29 and His199 were included. In addition, both peptide bonds were preserved in the amide form; that is, a COH moiety attached to the N-terminal side and an $NH_2$ moiety attached to the C-terminal side. The residue Asn219 was represented only by its side chain, with the Cα in methyl form. The coordinates of all main-chain atoms of Cys29 and His199 were kept frozen in all quantum chemistry calculations in order to preserve the enzyme conformation of the triad. The coordinates of Cα and Cβ in the Asn219 fragment were fixed with respect to the His199 imidazolium ring, maintaining the free movement of the amide moiety of Asn219. These systems were used for ionic-pair stability studies, which were done to gain some insight into the behavior of the triad under the modeling conditions and with the selected methodology. These quantum chemical calculations were performed at the DFT level using Gaussian09 [53]. The hybrid functional B3LYP [54–57] and the basis set 6-31++G** were chosen for this study.

The molecular systems employed for the mechanistic studies of thiadiazole were built using the complex of the *N*-(3-methoxy-1,2,4-thiadiazol-5-yl)-L-leucyl-L-proline methyl ester ligand (1) at the active site of CatB, derived from the docking studies, as the starting point. The systems included the catalytic triad and one molecule of the ligand. All possible protonation states of the ligand were assessed. These calculations were performed using the density functional theory with the hybrid B3LYP [54–57] and the meta-hybrid functional M06 [58], in both cases with the 6-31++G** basis set. The reason for using the M06 exchange-correlation potential is that it includes the kinetic energy in the functional, making it more accurate in general than B3LYP. It has been shown to be particularly useful for describing noncovalent interactions. Second derivatives of the energy with respect to the Cartesian coordinates of the optimized geometries were analyzed in order to confirm the character of each critical point.

## Results and discussion

### Receptor structure selection

Twenty crystallographic structures were retrieved from the RCSB Protein Data Bank (PDB) [46] and seven significant interatomic distances were measured in order to characterize the structure of the CatB active site. The results are shown in Table 1, where the distances are denoted according to the atoms involved and the residues to which those atoms belong (in parentheses). The table shows the average and standard deviation values for a group of eight structures grouped together under the label "1gmy type," the values for 1gmy itself, as well as the average and standard deviation values for a

**Scheme 1** The series of 1,2,4-thiadiazole derivatives modeled in the present work. Group A comprises the compounds that differ at the R1 position, while group B comprises the compounds that differ at the R2 position; note that (1) is included in both groups

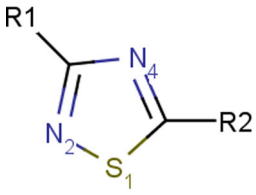


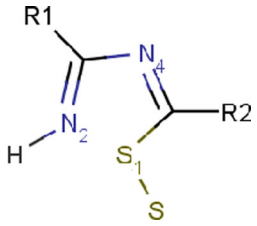


*Group A*

(1) R1 = MeO; R2 = -NH-Leu-Pro-OH

(2) R1 = phenyl; R2 = -NH-Leu-Pro-OH

(3) R1 = methyl; R2 = -NH-Leu-Pro-OH

(4) R1 = HOOC; R2 = -NH-Leu-Pro-OH

*Group B (including* (1)*)*

(5) R1 = MeO; R2 = -NHCONH-Leu-Pro-OH

(6) R1 = MeO; R2 = -NHCONH-Leu-isopentyl

(7) R1 = MeO; R2 = -NH-Phe-Cbz

(8) R1 = MeO; R2 = -NH-Ala-Phe-Cbz

group of nine structures identified as "2dcd type" and the values for 2dcd itself. Three structures presented special deviations and were not included in either of the types mentioned. The complete table can be consulted in the ESM.

The parameters presented in Table 1 allowed us to organize the twenty structures selected into two groups. Each group is associated with its representative PDB entry, either 1gmy or 2dcd. The former structure has been used in several docking studies since it being deposited at the PDB website. Most recently, it was referenced by Zhou et al. [33] and Sosič et al. [34]. Basically, the difference between these two structural types can be traced to the distance between Cα of Glu122 and Cα of Asn72, which is ca. 3 Å more in the 2dcd-type structures. This distance can be associated with the cleft of the S2′ subsite (see [59]), in which Glu122 is in the so-called occluding loop [9]. This flexible fragment is displaced in the 2dcd-type structures in order to allow the binding of the ligand (Fig. 1). While the crystallographic nitrile ligand of 1gmy does not occupy the S2′ sub-site (Fig. 1a), the epoxy-dipeptide ligand of 2dcd selectively occupies this region. As the thiadiazole ligands studied in this work have moieties that can bind in this region, then the 2dcd structure was initially chosen for the docking calculations. The 1gmy, 2dca, 2dcb, and 2dcc receptor structures were added to the study in order to take into account fluctuations of the active site. The selection aimed to include three extra situations in which the original ligand occupies the S2′ subsite and one situation (1gmy) in which the ligand does not.

The website of the Electron Density Server (EDS) [60] from Uppsala University, Sweden, was utilized to test the quality of the structures. For instance, the data for 2dcd were: resolution 2.50 Å, MapR of 0.194 $Å^2$, and an occupancy-weighted average temperature factor of 16.9 (7.4) $Å^2$. Although the Glu122 side-chain density is poorly resolved in the 2dcd series, the Ramachandran plot indicates that the main-chain Cα is in its normal position. Additionally, the side chain of this residue does not interact with the ligands, thus validating our decision to use these structures in the calculations. The residue Glu122 is correctly resolved in the 1gmy structure.

## Docking studies

Twenty complexes (solutions) were built for the complete series in each docking study: ten initial complexes and ten complexes that were constructed at the refinement stage. Table 2 shows the values obtained for each ligand in a noncovalent docking study and the experimentally derived kinetic constants [41]. For the eight compounds displayed, the dipeptide moiety selectively occupied the S1′ and S2′ subsites [58] in the five receptor structures studied, demonstrating a rational family pattern of binding as CatB inhibitors. In light of these results, it is possible to organize the analyses of the binding affinity into two sequences: those that differ at the R1 position (comparison A: compounds (1)–(4)), and those that differ at the R2 position (comparison B: compounds (1) and (5)–(8)). Comparison A did not show any clear correlation between the binding scores and the experimental kinetic constants. This can be rationalized by the assumption that R1 substitution mainly affects the electronic environment of the thiadiazole ring, and thus the reactivity of the ring compared with the global structural binding affinity. This position was named the "reactivity tuner" by Leung-Toung et al. [41]; as the substituent at this position controls ring opening. The location of this position in the complexes means that substituents at this position are exposed to the solvent in the outer region of the active site. In this case, the solvent may influence the final experimental free energy values, so the docking scores will not correctly reproduce the correlation. Moreover, the strength of the interaction between the sulfur

**Table 1** Interatomic distances used to characterize the structure of the CatB active site

| Structure(s) considered | Interatomic distance in Å (standard deviation is shown in parentheses) | | | | | | | |
|---|---|---|---|---|---|---|---|---|
| | O(Gly198)···N(His111) | N(His111)···C(Pro118) | C(Pro118)···Cα(Glu122) | Cα(Glu122)···Cα(Asn72) | Cα(Asn72)···Cα(Tyr75) | Cα(Tyr75)···Cα(Glu245) | Cα(Glu245)···O(Gly198) |
| 1gmy-type structures | 14.69 (0.38) | 7.11 (0.21) | 10.63 (0.30) | **6.53** (0.36) | 10.79 (0.07) | 10.18 (0.29) | 11.69 (0.34) |
| 1gmy | 15.07 | 7.03 | 10.71 | **6.55** | 10.82 | 9.57 | 11.09 |
| 2dcd-type structures | 14.67 (0.31) | 7.09 (0.05) | 10.19 (0.17) | **9.34** (0.26) | 10.77 (0.02) | 9.88 (0.09) | 11.86 (0.16) |
| 2dcd | 14.22 | 7.11 | 10.02 | **9.00** | 10.77 | 10.05 | 12.22 |

atom of the ligand and that of Cys29 is certainly influenced by the substituent at R1. This effect is not taken into account by the score equations used in this study.

This set of ligands is a family of eight active and very similar compounds, so it was a challenge to obtain a clear correlation between the calculated scores and the experimental kinetic constants. As these compounds are quite similar, the scoring equation—which is a summation of the optimized interactions—showed a tendency to increase the baseline of scoring values with an increasing number of atoms, and thus overestimate the scores for the larger compounds. This predisposition was also mentioned by Kitchen et al. [61]: "Large molecules can form many hypothetical interactions in binding sites and therefore have the tendency to generate better scores than smaller compounds." A similar difficulty was recently reported for a comparison of the scores for leupeptin and smaller ligands in CatB [62]. Therefore, we can define an "affinity index," which is the ChemPLP score divided by the total number of atoms, and use this to evaluate the overall affinities of these similar ligands. A slight correlation can be observed in comparison B when we compare the affinity indices (Table 2). Depending on the substituent moiety at the R2 position, the affinity indices follow the sequence (1)>(8)≥(7)>(6), which is similar to that seen for the constant $k$, and the same sequence (1)>(7)≥(8)>(6) is observed for the $K_d$ values (the lower the value of $K_d$, the higher the binding energy). Ligand (5) is very similar to (1) (but with an NHCO moiety inserted at the R2 position). From the point of view of docking studies, ligand (5) can be seen as a false positive, because it shows the second best affinity index but has the lowest experimental activity. No difference in docking results can be seen between the two tautomers tested for (1): the original ligand protonated at N6 and the ligand protonated at N3 (which is denoted in Table 2 as "(1)-T3").

The inhibition of CatB involves diverse effects ranging from noncovalent binding to covalent reactivity, so simulating it and correlating these theoretical results with their corresponding experimental values is a very challenging task. Despite this, combining different theoretical approximations can lead to a conceptual convergence towards a greater understanding of this complex mechanism.

## Noncovalent and covalent docking

The set of compounds was studied in two different situations: before and after the covalent inhibition of the catalytic cysteine. Therefore, two calculations were performed: a noncovalent docking (NCD) and a covalent docking (CD). In the latter, the disulfide bond formed between S1 in each compound and the SG of Cys29 was added to the ligand structure in order to satisfy the requirements of the program. In NCD, a single binding pattern binding was observed in which the distance between the sulfurs involved in the

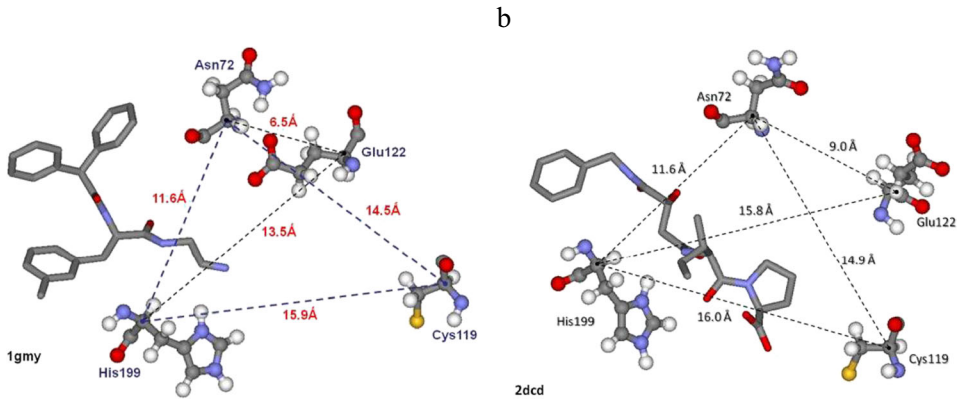


**Fig. 1a–b** Active-site region of CatB in the crystallographic structures of the complexes **a** 1gmy and **b** 2dcd. *Dashed lines* correspond to interatomic distances between the Cα atoms of representative residues

covalent inhibition was in the range 3–4 Å (Fig. 2). For (1), two samples were selected from this original calculation, both equivalent but with different orientations of the R1 methoxyl moiety with respect to the plane of the thiadiazole ring (mode1 and mode2). Both samples were refined by performing a new docking calculation using a scaffold constraint on one of the mentioned orientations. The docking solutions for mode1 refinement were all coherent with this orientation of the methoxyl moiety, whereas mode2 refinement showed both modes among its solutions, and a larger standard deviation for its score. The statistical weight of mode1 and its lower standard deviation for its score suggested that we should select this as the representative orientation. The same conclusion was reached from the CD solutions; in this docking study, 19 of the 20 complexes presented the mode1 conformation for the methoxyl moiety. Figure 2 shows the selected complexes for NCD and CD, both of which are in the mode1 conformation.

As seen in Table 3, the initial favorable interactions are fitted once covalent inhibition occurs (i.e., the interactions of N6 and O19). The final protonation state of N6, and its role in the mechanism, will be discussed later in the "Protonation states of ligand (1): reactivities of the tautomers" section. The bifurcated H-bond interaction of HE2_His111 in the NCD, derived in a more specific H-bond formed with O19 in the CD. The methoxyl moiety linked to the thiadiazole ring moved further away from Asn72 due to the increased S1···SG distance.

In the investigation of CatB inhibitors with micromolar $K_d$ values, good fitness is expected at the active site in noncovalent and covalent conditions. In other words, the ligand will show coherent conformations that can be accessed during the mechanism. No large structural torsions of the receptor and/or ligand are expected to be necessary. Unfortunately, when using docking methods, we only can study two stages that may or may not be connected by the sequence of events in the mechanism under investigation. If the ligand requires considerable structural adaptation to convert from the noncovalent to the covalent binding mode, this process will certainly be reflected in a less favorable free energy compared with ligands that show almost equivalent binding modes in both stages. The docking methods try to optimize the interactions in both situations, and thus tend to

**Table 2** Docking study results for ligands (1)–(8). The second to the sixth columns correspond to average ChemPLP scores over ten solutions. The seventh and eighth columns refer to the average ChemPLP scores over all 50 solutions (i.e., five receptor structures × ten each) and the corresponding the standard deviations. The remaining columns show the total number of atoms, the affinity index, the second-order kinetic constant $k$ ($M^{-1}$ $s^{-1}$) [41], and the noncovalent conversion constant $K_d$ (μM) [41], respectively

| Ligand | 2dcd | 2dca | 2dcb | 2dcc | 1gmy | Average | Std_dev | N_atm | Aff_idx | $k$[a] | $K_d$ |
|---|---|---|---|---|---|---|---|---|---|---|---|
| (1) | 64.65 | 57.20 | 54.34 | 47.97 | 52.45 | *55.32* | *5.55* | 44 | *1.2573* | 5630 | 2.6 |
| (2) | 65.83 | 65.01 | 60.71 | 55.03 | 57.44 | *60.80* | *4.19* | 50 | *1.2161* | 175 | 74 |
| (3) | 59.79 | 58.68 | 54.69 | 49.58 | 49.26 | *54.40* | *4.41* | 43 | *1.2651* | 55 | 446 |
| (4) | 58.45 | 57.47 | 52.57 | 47.76 | 50.47 | *53.34* | *4.08* | 42 | *1.2701* | 293 | 300 |
| (5) | 59.11 | 59.45 | 57.55 | 37.46 | 59.52 | *54.62* | *8.61* | 48 | *1.1379* | 36 | 390 |
| (6) | 43.29 | 48.84 | 49.94 | 41.73 | 35.74 | *43.91* | *5.15* | 51 | *0.8609* | 84 | 367 |
| (7) | 49.68 | 54.14 | 54.64 | 57.45 | 56.37 | *54.46* | *2.67* | 51 | *1.0678* | 658 | 21 |
| (8) | 59.48 | 64.11 | 62.66 | 62.02 | 58.31 | *61.32* | *2.12* | 61 | *1.0052* | 864 | 37 |
| (1)-T3 | 60.08 | 57.60 | 54.88 | 47.08 | 54.92 | *54.91* | *4.37* | 44 | *1.2480* | 5630[b] | 2.6[b] |

[a] $k=K_i/K_d$

[b] These are the same values as those presented in the first row

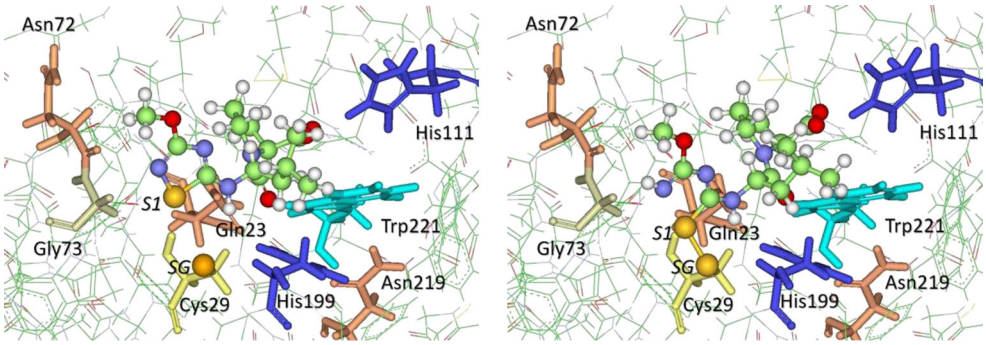


**Fig. 2** NCD complex of (1) mode1 (*left*) and CD complex of (1) mode1 (*right*) in the active site of CatB. Relevant residues are shown as sticks, ligands as balls and sticks, and the sulfur atoms that form the disulfide (S1 and SG) are depicted in both figures

overestimate the scores of dynamic processes that involve structural transformations. Table 4 presented the root mean square deviation (rmsd) values of each ligand in both situations (NCD and CD) in the receptor 2dcd. In the rmsd AS column, the values correspond to the superposition of the selected solutions at the active site. In the rmsd conf column, the values correspond to the alignment of both conformations. Only three ligands, with <25 non-H atoms, showed superpositions at the active site with rmsd AS values of <1.5 Å. These three ligands presented minor differences in the R1 substituent. When both conformations of these three ligands are aligned, the rmsd conf values decrease to ≤1 Å. Figures showing each ligand superposition at the active site in receptor 2dcd can be viewed in the ESM. For ligand (5), we performed a new NCD calculation using a scaffold constraint with the superposition of the previous CD conformation. In this case, the ChemPLP score decreased from ca. 60.0 for the free NCD to ca. 40.0 for the constrained NCD. This result suggests that the scores for ligands with considerable structural changes are overestimated.

As (1) was the most interesting inhibitor among the set (it presented good affinity indices and a reasonable fits and coherences in both conformations), we calculated the average GOLDScore for the 50 solutions obtained (10 solutions for each of 5 receptors). The average GOLDScore for the NCD of (1) is 52.22. If we use the empirical equation that estimates the free energy (in kJ mol$^{-1}$) from the GOLDScore value reported by Verdonk et al. [44]:

$$-\Delta G = (0.4502 \cdot \text{GoldScore} + 9.4891),$$

we obtain an estimated value of ca. −33.0 kJ mol$^{-1}$. If we estimate the free energy from the experimental $K_d$ value at 25 °C reported by Leung-Toung et al. [41], the value is −31.9 kJ mol$^{-1}$, i.e., in surprisingly good agreement with our estimated value. The other ligands are, in general, overestimated. (1) is a selective micromolar inhibitor and a ligand that showed good fitting and a regular pattern of binding in all of the docking calculations, so it seems to be a molecular complex that fits very well to those reported by Verdonk et al. [44].

## Protonation states of ligand (1): reactivities of the tautomers

The molecular systems were built according to the results from previous docking studies performed with the compound *N*-(3-methoxy-1,2,4-thiadiazol-5-yl)-L-leucyl-L-proline methyl ester (1) at the active site of CatB. All molecular systems included the catalytic triad Cys29, His199, and Asn219 (on behalf of the active site) as well as one molecule of the ligand. All possible protonation states were assessed (Fig. 3). All of the calculations were performed as mentioned in the

**Table 3** Selected ligand–protein distances (Å) for the NCD and CD complexes of (1)

| Interatomic distance | NCD mode1 | CD mode1 |
|---|---|---|
| S1···SG_Cys29 | 3.62 | 2.03[a] |
| N6···HE21_Gln23 | 3.20 | 2.36 |
| N6···HD1_His199 | 3.20 | 2.70 |
| C8–CG_Asn72 | 4.80 | 5.64 |
| O19···HE2_His111 | 2.54 | 1.81 |
| O20···HE2_His111 | 2.24 | 2.33 |

[a] This distance corresponds to a covalent disulfide bond

**Table 4** Root mean square deviations (Å) between the selected conformations during NCD and CD into the 2dcd structure. For each ligand, the columns represent the rmsd of the superposition at the active site (rmsd AS), the rmsd of the alignment of both conformations (rmsd conf), and the total number of non-H atoms considered (N atm)

| Ligand | rmsd AS | rmsd conf | N atm |
|---|---|---|---|
| (1) | 1.497 | 1.012 | 23 |
| (2) | 2.745 | 1.954 | 27 |
| (3) | 1.043 | 0.698 | 22 |
| (4) | 1.205 | 0.892 | 24 |
| (5) | 1.960 | 1.345 | 26 |
| (6) | 2.168 | 1.822 | 24 |
| (7) | 2.502 | 2.206 | 29 |
| (8) | 3.642 | 3.099 | 34 |

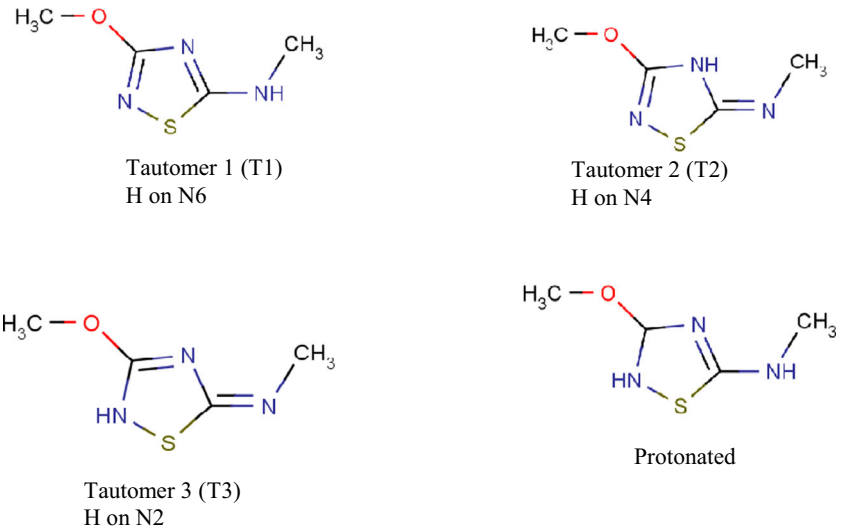


**Fig. 3** The four protonation states of (1) studied in this section

"Materials and methods" section, and the optimized geometries were analyzed by means of vibrational frequency calculations.

*Tautomer 1 (T1)*

The optimized geometry of the T1 system (see Fig. 4) reached a conformation in which the thiolate is involved in a hydrogen bond with N6 (2.469 Å) and the distance between both sulfur atoms is 4.217 Å. When the starting model (related to the docked conformation) was compared with the optimized one, a $\Delta E$ value of about 10 kcal mol$^{-1}$ was observed.

The mechanism suggested by Leung-Toung et al. [41] requires the protonation of N2 to enable ring opening. In previous calculations, we observed that this condition is necessary for the ring to remain open, so this system can be associated with a previous instant during the noncovalent inhibition stage.

*Protonated form*

The geometry of the system with the ligand in the protonated form (see Fig. 5) optimized to a conformation in which the thiolate achieves a position in which it simultaneously displays a hydrogen bond with N6 (2.286 Å) and an interaction with S1 (2.978 Å).

However, this does not result in the opening of the thiadiazole ring—the proximity of the imidazolium ring (His199) leads to a repulsion between both positive charges that appears to prevent the nucleophilic attack. One of the H atoms (associated with either N6 or His199) must be lost to enable both sulfurs to approach closely enough to form the disulfide. A $\Delta E$ value of approximately 7 kcal mol$^{-1}$ between the initial reference conformation and the final optimized conformation was noted for this process.

*Tautomer 2 (T2)*

The geometry of the T2 system (see Fig. 6) optimized to a conformation in which the salt bridge thiolate(−1)–imidazolium(+1) is maintained while the ligand moves away from the reactive pair, reaching a distance S–S of 6.894 Å in the step at which the calculation was stopped. The $\Delta E$ of this process was >20 kcal mol$^{-1}$.

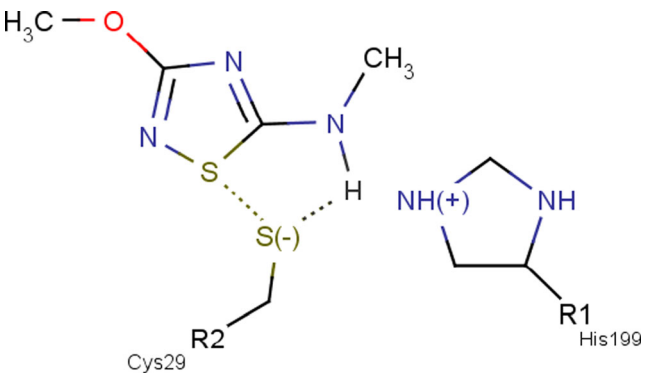


**Fig. 4** Schematic representation of the T1 molecular system

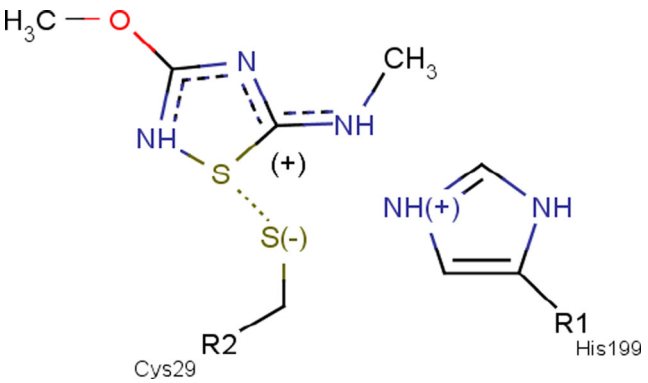


**Fig. 5** Schematic representation of the protonated molecular system

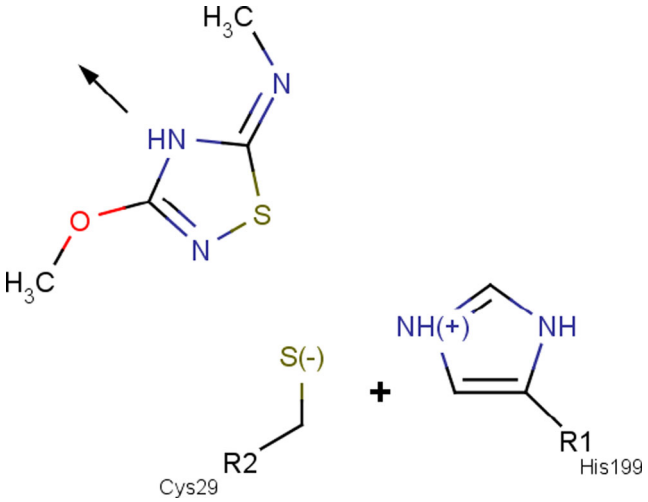


**Fig. 6** Schematic representation of the T2 molecular system

*Tautomer 3 (T3)*

The optimization of T3 involved three steps in a possible mechanism for the inhibition reaction (Fig. 7). The neutral ligand initially receives a positive charge from the imidazolium ring through the transfer of a proton to N6. The protonated ligand then stabilizes by forming a hydrogen bond with the imidazole ring. The sulfur slowly approaches the thiolate until, finally, the nucleophilic attack is completed, leading to a disulfide bond and the neutralization of the whole molecular system. The structural evolution is shown in Fig. 7, along with $\Delta E$ values that represent the differences in electronic energy between selected steps during the optimization.

The structural evolution of the T3 system during the sequence of events observed is in accord with experimental data on the inhibition mechanism, in which Cys29 ends up covalently bound to the ligand's sulfur.

As a consequence of these results, new docking calculations of (1) were performed using the T3 tautomer form as ligand. As mentioned in the "Noncovalent and covalent docking" section, no significant differences were observed, so we can presume that at the docking level of approximation employed in the molecular mechanics theory, the resolution of this system is not sufficient to be able to distinguish among tautomers.

The energy differences between the steps considered in the mechanism were confirmed using the M06 functional, which gave similar results to the previous calculations. The relative increase in energy obtained using the M06 potential in the three steps considered in Fig. 7 is slightly higher. The largest difference between the results obtained with both functionals is observed for the crucial step in which the TDZ ring opens, thus enabling the formation of the disulfide bond. This energy difference amounts to about 60 % of the total energy difference between the potentials for the whole process. Two graphics (Fig. 8) were constructed to analyze the structural

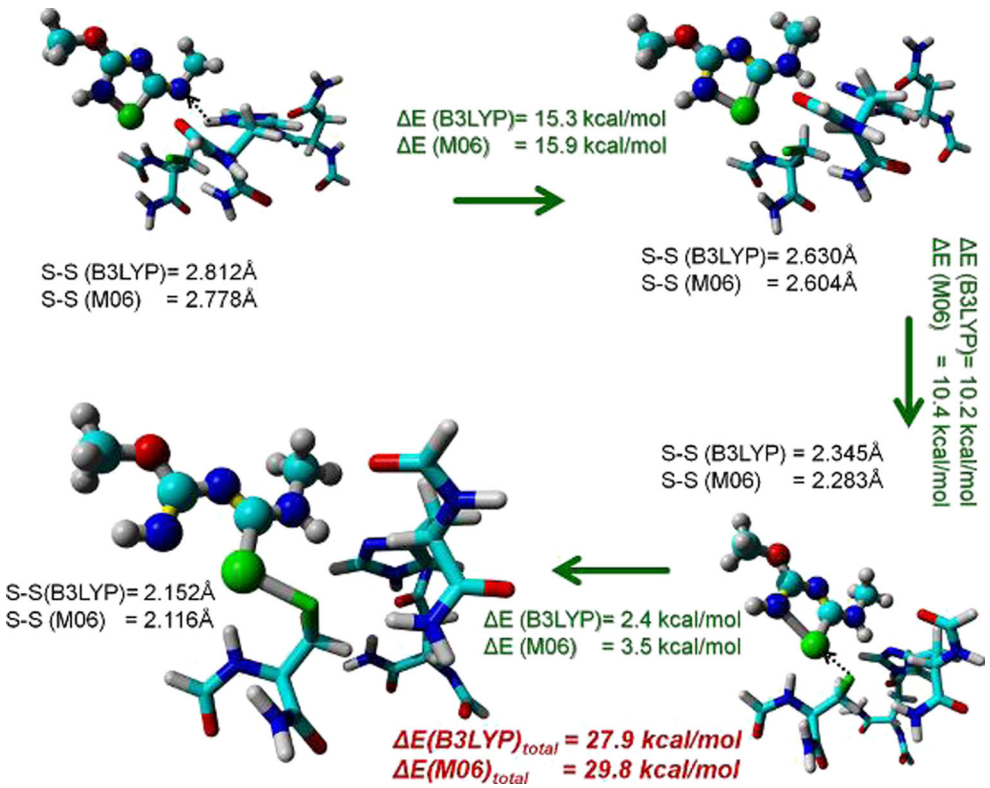


**Fig. 7** The four stages of the structural transformation during the process. The calculation was replicated using two different functionals, B3LYP and M06

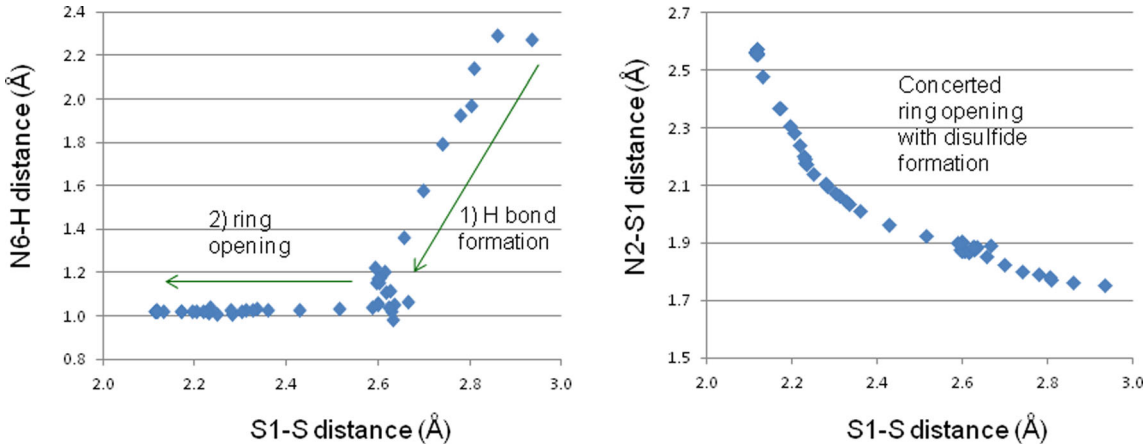


**Fig. 8** Graphics showing changes in particular interatomic distances (N6–H and S1–S) during the process of molecular transformation (*left*) and thiadiazole ring opening (*right*)

events that occurred during the process described in this section. When the sequence of structures that were generated during the energy optimization was evaluated with the aid of the intermolecular distances N6–H (from His199) and S1–S (from Cys29), the process was found to be divisible into two steps: an initial H transfer and H-bond formation during which the distance between the sulfurs decreases; then, with the H bonded to the ligand (charge+), the S of the thiolate attacks S1 of the thiadiazole ring. When this sequence is evaluated with the aid of the interatomic distances N2–S1 and S1–S, it becomes clear that the process can be described as a concerted ring opening that occurs at the same time as disulfide bond formation.

The system T3 was tested under several dielectric conditions (from heptane to water) using the PCM (polarizable continuum model) [63] to analyze the sequence of events observed in vacuum in environments close to those present inside the enzyme. In this procedure, we tried to simulate different medium conditions at the active site. Even when the more hydrophobic model was tested (heptane: $\varepsilon$=1.92), the protonation of N6 did not occur (first stage in Fig. 7). When the initial model was protonated manually (second stage in Fig. 7), the evolution of the system was the same under vacuum conditions for the dielectric constant (heptane, $\varepsilon$=1.92; ether, $\varepsilon$=4.34; chlorobenzene, $\varepsilon$=5.62; aniline, $\varepsilon$=6.89) with the final stage shown in Fig. 7 attained. When the model was tested using quinoline ($\varepsilon$=9.03), the disulfide did not form (third stage in Fig. 7). However, when we optimized the structure with the disulfide and the open ring (final stage in Fig. 7), the system showed stability even in aqueous conditions ($\varepsilon$=78.39), indicating that the final product can be achieved in this environment too. In light of these results, we can conceive that, under enzymatic conditions, the mechanism involves an initial energy barrier to the protonation of the ligand. This is in accord with the mechanism proposed for cysteine proteases, which involves the transfer of a proton from His199 to the natural substrate [14]. Disulfide formation without an intermediate state is feasible up to $\varepsilon$~7, a condition that may be expected in the internal hydrophobic active sites found in these enzymes. This confirmation that the system with the disulfide is stable even under aqueous conditions demonstrates the reliability of the simulation. The energy barrier to ligand protonation was estimated for the system described in the next section.

## Ligand (1) inhibition mechanism

In a final study, a new model comprising 140 atoms was constructed. The ligand was modeled in the T3 tautomeric form with the carboxylic terminus neutralized to preserve the overall neutrality of the system. The active site of the enzyme was represented by adding two residues: the fragment of Asn72 with both peptidic bonds included as part of the main chain, and the side chain of Gln23. The former is associated with the stabilization of N2 and the methoxy substituent of the ring, and the latter with the stabilization of the Pro moiety of the ligand and the residues Cys29 and His199.

As can be seen in Fig. 9, the mechanism for Cys29 inhibition unfolds in a similar manner to the corresponding mechanism seen for the smaller systems. With a more complete representation of the active site, an activation step was observed in which there was a small barrier of ca. 15 kcal $mol^{-1}$ to proton transfer (Fig. 10), in contrast to the mechanism observed in vacuum for the smaller systems. The barrier was estimated by fixing the overall structure and scanning the dihedral value of the proton in relation to Cys29, relaxing its position at every step. This modeling procedure allowed us to simulate the transfer of the proton in the space between NE of His199 and N6 of the ligand. The energy profile for the complete evolution of the system can be observed in Fig. 10.

The evolution of the system involves a small barrier to proton transfer (Fig. 10a–b). After that, the protonated ligand inserts into the active site, leading to a very low shoulder in the

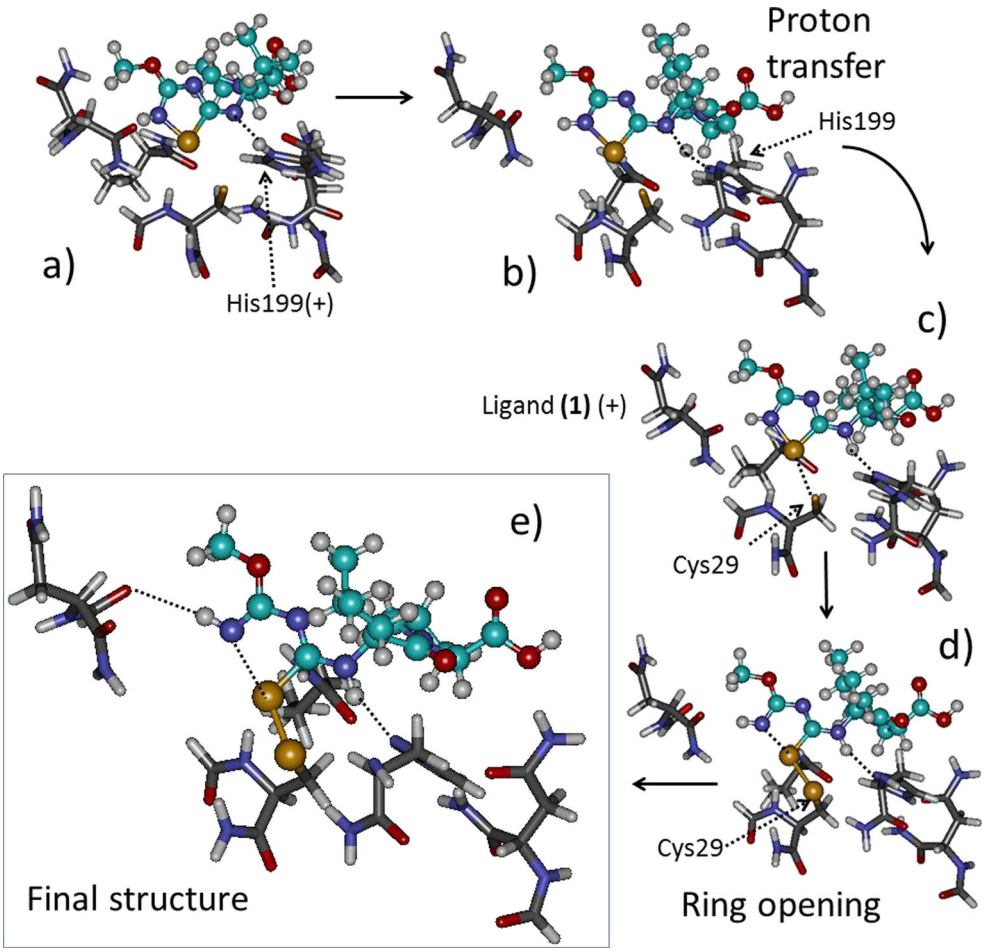


**Fig. 9a–e** Structural evolution of the system with 140 atoms. **a** His199 in the protonated state. **b** Proton transfer to the ligand. **c** Protonated ligand. **d** TDZ ring opening. **e** Final structure of the neutralized system

energy profile (Fig. 10c–d) which is associated with the formation of the disulfide and simultaneous ring opening. At the end of the curve, the system has adopted its optimized final structure. Table 5 presents intra- and interatomic distances for the optimized neutral ligand, protonated ligand, and the optimized bound ligand, including the final distance between the sulfur atoms in the (disulfide ligand)–Cys29 bridge (2.138 Å).

In light of these results, we postulate that the protonated His199 acts as a trigger to convert the inhibitor molecule into a

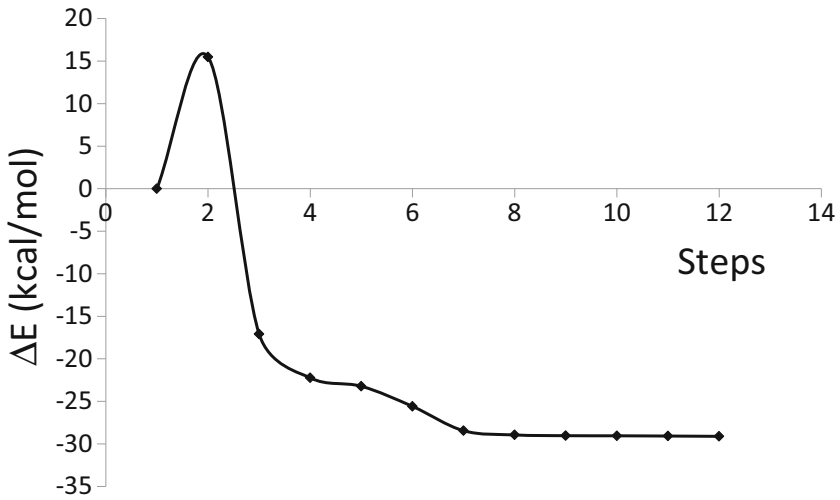


**Fig. 10** Energy profile (kcal/mol) for the complete evolution of the system (12 selected steps) from the optimized neutral ligand to the optimized final structures, including the formation of the (disulfide ligand)–Cys29 bridge. The letters *a–e* correspond to the stages shown in Fig. 9

**Table 5** H-bond lengths and interatomic distances (Å) for the optimized neutral ligand, protonated ligand (with the ring closed), and the bound ligand (with the (disulfide ligand)–Cys29 bridge formed)

| | Neutral ligand | Protonated ligand | Bound ligand |
|---|---|---|---|
| Intramolecular distances in CatB | | | |
| OE_Gln23···HB1_Cys29 | 2.882 | 2.902 | 2.912 |
| OE_Gln23···HCE_His199 | 2.696 | 2.691 | 2.768 |
| HNE_His199···OD–Asn219 | 1.734 | 1.809 | 1.811 |
| Intermolecular distances (ligand···CatB) | | | |
| S1···SG_Cys29 (disulfide) | 2.850 | 2.486 | 2.138 |
| N6···H–ND_His199 | 1.958 | 1.035[a] | 1.029[a] |
| O_Pro···HND_Asn219 | 2.156 | 2.221 | 2.203 |
| HCD_Pro···NE_Gln23 | 2.806 | 2.662 | 2.628 |
| N1–H···O_Gly72 | 3.179 | 3.045 | 2.758 |
| HMe···O_His199 | 2.673 | 2.480 | 2.543 |

[a] The H bond N6···H becomes a covalent bond and vice versa

more electrophilic target for the thiolate form of Cys29. This function of donating a proton to the protein chain of a natural substrate has already been assigned to His199 in the protease literature [14].

## Conclusions

The search for and optimization of potent inhibitors of CatB and other cysteine proteases that provide therapeutic targets is a research field in which any new information is most welcome. The application of docking methods to thiadiazole derivatives and related compounds in CatB is a valuable approach considering the high quality of the theoretical complexes generated. The statistical values and affinity indices derived from multiple solutions for multiple receptor structures appear to be more useful than the best score value obtained unless the structure associated with this score is clearly the solution selected to represent the complex inhibitor–CatB model. When using docking methods for virtual screening or to study the docking of a specific family of ligands into CatB, it is important to consider the potential difficulties when the number of atoms exceeds 45–50. The conformations obtained with both NCD and CD should be compared, and it should be checked that both show good superpositions at the active site. This procedure can help to avoid the score overestimation observed for ligands with poor selectivity or those that require considerable torsion. Ligands that present behavior similar to that observed for (1), a good affinity index, adequate fits of the NCD and CD conformations at the active site, and reproducibility in the mode and pattern of binding for several receptor structures are expected to be candidates for experimental tests.

Combining docking and quantum chemistry calculations allowed us to adequately model the systems and to evaluate the structural and electronic events with the ligand in its correct orientation (i.e., the orientation that the active site imposes on the ligand). The calculations pointed to a sequence of structural events that is initiated by the transfer of a proton from the charged His199 residue to the ligand. The results of this work are expected to aid the development of new inhibitors of cysteine proteases through virtual screening as they enhance our theoretical understanding of the electronic conditions needed for disulfide formation and simultaneous opening of the thiadiazole ring.

**Acknowledgments** MVT is grateful to Conselho Nacional de Desenvolvimento Científico e Tecnologia-CNPq (473265/2008-7) and the Center for Scientific Computing (NCC/GridUNESP) of São Paulo State University (UNESP) for the computational resources they supplied. MVT and ONV are thankful to Comisión Sectorial de Investigación Científica-CSIC (CSIC/655), Programa de Desarrollo de las Ciencias Básicas-PEDECIBA, and Agencia Nacional de Investigación e Innovación-ANII. JRS, SChM (09/52188-8), and CBR (09/52189-4) are grateful to Fundação de Amparo à Pesquisa do Estado de São Paulo-FAPESP.

## References

1. Buttle DJ, Saklatvala J, Barret AJ (1993) The inhibition of interleukin 1-stimulated cartilage proteoglycan degradation by cysteine endopeptidase inactivators. Agents Action Suppl 39:161–165
2. Delaisse JM, Pascale L, Vaes G (1991) Collagenolytic cysteine proteinases of bone tissue. Cathepsin B, (pro)cathepsin L and a cathepsin L-like 70 kDa proteinase. Biochem J 279:167–174
3. Katunuma N, Kominami E (1987) Abnormal expression of lysosomal cysteine proteinases in muscle wasting diseases. Rev Physiol Biochem Pharmacol 108:1–20
4. Turk V, Stoka V, Vasiljeva O, Renko M, Sun T, Turk B, Turk D (2012) Cysteine cathepsins: from structure, function and regulation to new frontiers. Biochim Biophys Acta 1824:68–88
5. Naudin C, Lecaille F, Chowdhury S, Krupa JC, Purisima E, Mort JS, Lalmanach G (2010) The occluding loop of cathepsin B prevents its effective inhibition by human kininogens. J Mol Biol 400:1022–1035
6. Rawlings ND, O'Brien E, Barrett AJ (2002) MEROPS: the protease database. Nucleic Acids Res 30:343–346

7. Rawlings ND, Morton FR, Barrett AJ (2006) MEROPS: the peptidase database. Nucleic Acids Res 34:D270–D272
8. Stoeckle C, Gouttefangeas C, Hammer M, Weber E, Melms A, Tolosa E (2009) Cathepsin W expressed exclusively in $CD8^+$ T cells and NK cells, is secreted during target cell killing but is not essential for cytotoxicity in human CTLs. Exp Hematol 37:266–275
9. Illy C, Quraishi O, Wang J, Purisima E, Vernet T, Mort JS (1997) Role of the occluding loop in cathepsin B activity. J Biol Chem 272: 1197–1202
10. Nagler DK, Storer AC, Portaro FC, Carmona E, Juliano L, Ménard R (1997) Major increase in endopeptidase activity of human cathepsin B upon removal of occluding loop contacts. Biochemistry 36:12608–12615
11. Podobnik M, Kuhelj R, Turk V, Turk D (1997) Crystal structure of the wild-type human procathepsin B at 2.5 Å resolution reveals the native active site of a papain-like cysteine protease zymogen. J Mol Biol 271:774–788
12. Polgár L, Halász P (1982) Current problems in mechanistic studies of serine and cysteine proteinases. Biochem J 207:1–10
13. Menard R, Storer AC (1992) Oxyanion hole interactions in serine and cysteine proteases. Biol Chem Hoppe Seyler 373:393–400
14. Lecaille F, Kaleta J, Bröme D (2002) Human and parasitic papain-like cysteine proteases: their role in physiology and pathology and recent developments in inhibitor design. Chem Rev 102:4459–4488
15. Brix K, Dunkhorst A, Mayer K, Jordans S (2008) Cysteine cathepsins: cellular roadmap to different functions. Biochimie 90:194–207
16. Buck MR, Karustis DG, Day NA, Honn KV, Sloane BF (1992) Degradation of extracellular-matrix proteins by human cathepsin B from normal and tumour tissues. Biochem J 282:273–278
17. Bever CT Jr, Gaver DW (1995) Increased cathepsin B activity in multiple sclerosis brain. J Neurol Sci 131:71–73
18. Irani DN, Anderson C, Gundry R, Cotter R, Moore S, Kerr DA, McArthur JC, Sacktor N, Pardo CA, Jones M, Calabresi PA, Nath A (2006) Cleavage of cystatin C in the cerebrospinal fluid of patients with multiple sclerosis. Ann Neurol 59:237–247
19. Otto HH, Schirmeister T (1997) Cysteine proteases and their inhibitors. Chem Rev 97:133–171
20. Dawra R, Delori LR, Bekolay A, Sah RP, Saluja AK (2010) Deletion of cationic trypsinogen or cathepsin B gene in mice does not influence caerulein induced activation of Nfkb in pancreas. Pancreas 39(8):1317–1318
21. Hook V, Toneff T, Bogyo M, Medzihradszky KF, Neveu J, Lane W, Hook G, Reisine T (2005) Inhibition of cathepsin B reduces β-amyloid production in regulated secretory vesicles of neuronal chromaffin cells: evidence for cathepsin B as a candidate β-secretase of Alzheimer's disease. Biol Chem 386:931–940
22. Hook V, Lydiane Funkelstein L, Wegrzyn J, Bark S, Kindy M, Hook G (2012) Cysteine cathepsins in the secretory vesicle produce active peptides: cathepsin L generates peptide neurotransmitters and cathepsin B produces beta-amyloid of Alzheimer's disease. Biochim Biophys Acta 1824:89–104
23. Sundelof J, Sundstrom J, Hansson O, Eriksdotter-Jonhagen M, Giedraitis V, Larsson A, Degerman-Gunnarsson M, Ingelsson M, Minthon L, Blennow K, Kilander L, Basun H, Lannfelt L (2010) Higher cathepsin B levels in plasma in Alzheimer's disease compared to healthy controls. J Alzheimers Dis 22:1223–1230
24. Withana NP, Blum G, Sameni M, Slaney C, Anbalagan A, Olive MB, Bidwell BN, Edgington L, Wang L, Moin K, Sloane BF, Anderson RL, Bogyo MS, Parker BS (2012) Cathepsin B inhibition limits bone metastasis in breast cancer. Cancer Res 72:1199–1209
25. Chan AT, Baba Y, Shima K, Nosho K, Chung DC, Hung KE, Mahmood U, Madden K, Poss K, Ranieri A, Shue D, Kucherlapati R, Fuchs CS, Ogino S (2010) Cathepsin B expression and survival in colon cancer: implications for molecular detection of neoplasia. Cancer Epidemiol Biomarkers Prev 19:2777–2785
26. Diederich S, Sauerhering L, Weis M, Altmeppen H, Schaschke N, Reinheckel T, Erbar S, Maisner A (2012) Activation of the Nipah virus fusion protein in MDCK cells is mediated by cathepsin B within the endosome-recycling compartment. J Virol 86:3736–3745
27. Renko M, Požgan U, Majera D, Turk D (2010) Stefin A displaces the occluding loop of cathepsin B only by as much as required to bind to the active site cleft. FEBS J 277:4338–4345
28. Costa MGS, Batista PR, Shida CS, Robert CH, Bisch PM, Pascutti PG (2010) How does heparin prevent the pH inactivation of cathepsin B? Allosteric mechanism elucidated by docking and molecular dynamics. BMC Genomics 11(5):S5
29. Tomoo K (2010) Development of cathepsin inhibitors and structure-based design of cathepsin B-specific inhibitor. Curr Top Med Chem 10:696–707
30. Fukushima K, Arai M, Kohno Y, Suwa T, Satoh T (1990) An epoxysuccinic acid derivative(loxistatin)-induced hepatic injury in rats and hamsters. Toxicol Appl Pharmacol 105:1–12
31. McKerrow JH, Engel JC, Caffrey CR (1999) Cysteine protease inhibitors as chemotherapy for parasitic infections. Bioorg Med Chem 7:639–644
32. Bethel PA, Gerhardt S, Jones EV, Kenny PW, Karoutchi GI, Morley AD, Oldham K, Rankine N, Augustin M, Krapp S, Simader H, Steinbacher S (2009) Design of selective cathepsin inhibitors. Bioorg Med Chem Lett 19:4622–4625
33. Zhou Z, Wang Y, Bryant SH (2011) Multi-conformation 3D QSAR study of benzenesulfonyl-pyrazol-ester compounds and their analogs as cathepsin B inhibitors. J Mol Graph Model 30:135–147
34. Sosič I, Mirković B, Turk S, Štefane B, Kos J, Gobec S (2011) Discovery and kinetic evaluation of 6-substituted 4-benzylthio-1,3,5-triazin-2(1*H*)-ones as inhibitors of cathepsin B. Eur J Med Chem 46:4648–4656
35. Casini A, Gabbiani C, Sorrentino F, Rigobello MP, Bindoli A, Geldbach TJ, Marrone A, Re N, Hartinger CG, Dyson PJ, Messori L (2008) Emerging protein targets for anticancer metallodrugs: inhibition of thioredoxin reductase and cathepsin B by antitumor ruthenium(II)-arene compounds. J Med Chem 51:6773–6781
36. Mirković B, Renko M, Turk S, Sosič I, Jevnikar Z, Obermajer N, Turk D, Gobec S, Kos J (2011) Novel mechanism of cathepsin B inhibition by antibiotic nitroxoline and related compounds. ChemMedChem 6:1351–1356
37. Mirković B, Sosič I, Gobec S, Kos J (2011) Redox-based inactivation of cysteine cathepsins by compounds containing the 4-aminophenol moiety. PLoS ONE 6(11):e27197
38. Cunha RLOR, Gouvêa IE, Feitosa GPV, Alves MFM, Brömme D, Comasseto JV, Tersariol ILS, Juliano L (2009) Irreversible inhibition of human cathepsins B, L, S and K by hypervalent tellurium compounds. Biol Chem 390:1205–1212
39. Caracelli I, Vega-Teijido M, Zukerman-Schpector J, Cezari MHS, Lopes JGS, Juliano L, Santos PS, Comasseto JV, Cunha RLOR, Tiekink ERT (2012) A tellurium-based cathepsin B inhibitor: molecular structure, modelling, molecular docking and biological evaluation. J Mol Struct 1013:11–18
40. Murayama S, Imae Y, Takada K, Kikuchi J, Nakao Y, van Soest RWM, Okada S, Matsunaga S (2011) Shishicrellastatins, inhibitors of cathepsin B, from the marine sponge *Crella* (*Yvesia*) *spinulata*. Bioorg Med Chem 19:6594–6598
41. Leung-Toung R, Wodzinska J, Li W, Lowrie J, Kukreja R, Desilets D, Karimian K, Tam TF (2003) 1,2,4-Thiadiazole: a novel cathepsin B inhibitor. Bioorg Med Chem 11:5529–5537
42. Jones G, Willett P, Glen RC (2005) Molecular recognition of receptor sites using a genetic algorithm with a description of desolvation. J Mol Biol 245:43–53
43. Jones G, Willett P, Glen RC, Leach AR, Taylor R (1997) Development and validation of a genetic algorithm for flexible docking. J Mol Biol 267:727–748

44. Verdonk ML, Cole JC, Hartshorn MJ, Murray CW, Taylor RD (2003) Improved protein–ligand docking using GOLD. Proteins 52:609–623
45. Clark M, Cramer RD, Van Opdenbosch N (1989) Validation of the general purpose Tripos 5.2 forcefield. J Comput Chem 10:982–1012
46. Research Collaboratory for Structural Bioinformatics (2014) Protein Data Bank. http://www.rcsb.org/pdb/
47. Korb O, Stützle T, Exner TE (2009) Empirical scoring functions for advanced protein–ligand docking with PLANTS. J Chem Inf Model 49:84–96
48. Greenspan PD, Clark KL, Tommasi RA, Cowen SD, McQuire LW, Farley DL, van Duzer JH, Goldberg RL, Zhou H, Du Z, Fitt JJ, Coppa DE, Fang Z, Macchia W, Zhu L, Capparelli MP, Goldstein R, Wigg AM, Doughty JR, Bohacek RS, Knap AK (2001) Identification of dipeptidyl nitriles as potent and selective inhibitors of cathepsin B through structure-based drug design. J Med Chem 44:4524–4534
49. Watanabe D, Yamamoto A, Matsumoto K, Murata M, Kitamura K, Tomoo K, Ishida T (2006) Quantitative evaluation of each catalytic subsite of cathepsin B for inhibitory activity based on inhibitory activity-binding mode relationship of epoxysuccinyl inhibitors by X-ray crystal structure analyses of complexes. J Mol Biol 362:979–993
50. Accelrys Software Inc. (2007) Discovery Studio Modeling Environment, release v2.5.5.9350. Accelrys Software Inc., San Diego
51. Stewart JJP (2008) MOPAC2009. Stewart Computational Chemistry, Colorado Springs. http://OpenMOPAC.net
52. Stewart JJP (2007) Optimization of parameters for semiempirical methods V: modification of NDDO approximations and application to 70 elements. J Mol Model 13:1173–1213
53. Frisch MJ, Trucks GW, Schlegel HB, Scuseria GE, Robb MA, Cheeseman JR, Scalmani G, Barone V, Mennucci B, Petersson GA, Nakatsuji H, Caricato M, Li X, Hratchian HP, Izmaylov AF, Bloino J, Zheng G, Sonnenberg JL, Hada M, Ehara M, Toyota K, Fukuda R, Hasegawa J, Ishida M, Nakajima T, Honda Y, Kitao O, Nakai H, Vreven T, Montgomery Jr JA, Peralta JE, Ogliaro F, Bearpark M, Heyd JJ, Brothers E, Kudin KN, Staroverov VN, Kobayashi R, Normand J, Raghavachari K, Rendell A, Burant JC, Iyengar SS, Tomasi J, Cossi M, Rega N, Millam JM, Klene M, Knox JE, Cross JB, Bakken V, Adamo C, Jaramillo J, Gomperts R, Stratmann RE, Yazyev O, Austin AJ, Cammi R, Pomelli C, Ochterski JW, Martin RL, Morokuma K, Zakrzewski VG, Voth GA, Salvador P, Dannenberg JJ, Dapprich S, Daniels AD, Farkas Ö, Foresman JB, Ortiz JV, Cioslowski J, Fox DJ (2009) Gaussian 09, revision A.1. Gaussian, Inc., Wallingford
54. Becke AD (1993) Density-functional thermochemistry. III. The role of exact exchange. J Chem Phys 98:5648–5652
55. Lee C, Yang W, Parr RG (1988) Development of the Colle–Salvetti correlation–energy formula into a functional of the electron density. Phys Rev B 37:785–789
56. Vosko SH, Wilk L, Nusair M (1980) Development of the Colle–Salvetti correlation–energy formula into a functional of the electron density. Can J Phys 58:1200–1211
57. Stephens PJ, Devlin FJ, Chabalowski CF, Frisch MJ (1994) Ab initio calculation of vibrational absorption and circular dichroism spectra using density functional force fields. J Phys Chem 98:11623–11627
58. Zhao Y, Truhlar DG (2008) The M06 suite of density functionals for main group thermochemistry, thermochemical kinetics, noncovalent interactions, excited states, and transition elements: two new functionals and systematic testing of four M06-class functionals and 12 other functionals. Theor Chem Account 120:215–241
59. Schechter I, Berger A (1967) On the size of the active site in proteases. I. Papain. Biochem Biophys Res Commun 27:157–162
60. Kleywegt GJ, Harris MR, Zou JY, Taylor TC, Wählby A, Jones TA (2004) The Uppsala Electron-Density Server. Acta Cryst D 60:2240–2249. http://eds.bmc.uu.se/eds
61. Kitchen DB, Decornez H, Furr JR, Bajorath J (2004) Docking and scoring in virtual screening for drug discovery: methods and applications. Nat Rev Drug Discov 3:935–949
62. Raghav N, Singh M (2014) Design, synthesis and docking studies of bischalcones based quinazoline-2(1*H*)-ones and quinazoline-2(1*H*)-thiones derivatives as novel inhibitors of cathepsin B and cathepsin H. Eur J Pharm Sci 54:28–39. doi:10.1016/j.ejps.2013.12.018
63. Tomasi J, Mennucci B, Cammi R (2005) Quantum mechanical continuum solvation models. Chem Rev 105:2999–3093